Artificial Neural Networks-Based Multi-Objective Design Methodology for Wide-Bandgap Power Electronics Converters

RAJESH RAJAMONY[1], SHENG WANG [1] (Member, IEEE), GERARDO CALDERON-LOPEZ [2], INGO LUDTKE [2], AND WENLONG MING [1,2] (Member, IEEE)

[1]Department of Electrical and Electronic Engineering, School of Engineering, Cardiff University, CF24 3AA Cardiff, U.K.
[2]Compound Semiconductor Applications Catapult, NP10 8BE Newport, U.K.

CORRESPONDING AUTHOR: WENLONG MING (e-mail: wenlongming@ieee.org)

ABSTRACT Design methodology of power electronics converters is critical to fully explore the potential of wide-bandgap power semiconductors at the converter level. However, existing design methods largely rely on complex mathematical models which significantly increases the computational time, complexity and further leads to problems including poor constraint handling capabilities, inaccurate design, difficult parameter tuning and inadequate problem dimension. These all could generate sub-optimal designs that make the whole design process meaningless. To overcome the aforementioned problems, in this paper, an artificial neural network (ANN)-based multi-objective design approach is proposed, which offers significant advantages in reducing the repetitive usage of complex mathematical models and hence the computational time of design. The computational time was reduced by up to around 78% and 67% compared to the numerical modeling and geometric program (GP) methods as validated through a hardware design process. The proposed method was implemented in MATLAB/Simulink to design a 1 kW single-phase inverter, resulting in a design with an optimized efficiency (98.4%) and power density (4.57 kW/dm^3). The accuracy of the design is verified through experimental prototyping and the measured efficiency and power density are 98.02% and 4.54 kW/dm^3, respectively, so the errors of efficiency and power density are both less than 1%.

INDEX TERMS Artificial neural network, multi-objective design, single-phase inverter, efficiency, power density.

I. INTRODUCTION

The design of power electronic converters should consider mutually coupled performance parameters including efficiency, power density, cost, and reliability, as given in Fig. 1 [1]. A well-designed power electronic converter will have high efficiency, small volume, light weight, low cost, and low failure rate. However, the challenge is the trade-off due to the mutually coupled performance parameters, e.g., a design focused only on maximizing efficiency will inevitably sacrifice the power density, reliability, and cost of the converter. In Fig. 1, the texts in red are factors that primarily affect converter performance. For instance, the switching frequency mainly affects the efficiency and volume. Such factors include switching frequency, level of integration, derating redundancy, inverter complexity, redundancy, and initial and life cycle costs. The trade-offs mainly depend on the factors including converter topology, modulation scheme of power switches, converter components, and design layout [2]. By carrying out careful design, the converter will have high power density, and reduced volume, weight, and cost. Therefore, the main goal of a converter design method is to identify the best trade-off among multiple performances.

The design methods are broadly classified into traditional methods, and optimization methods, as shown in Fig. 2. The analytical method is one of the traditional methods, which is derived based on the analytical equations of the power
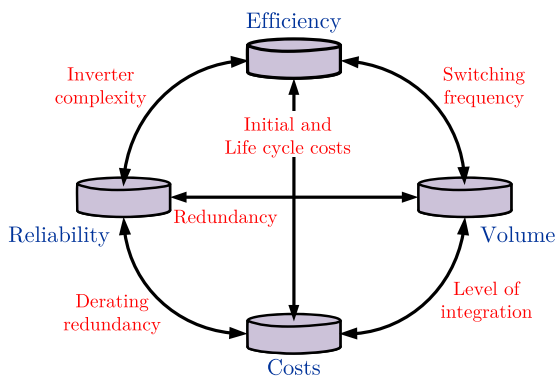
FIGURE. 1. Trade-off between the power electronic performance parameters.
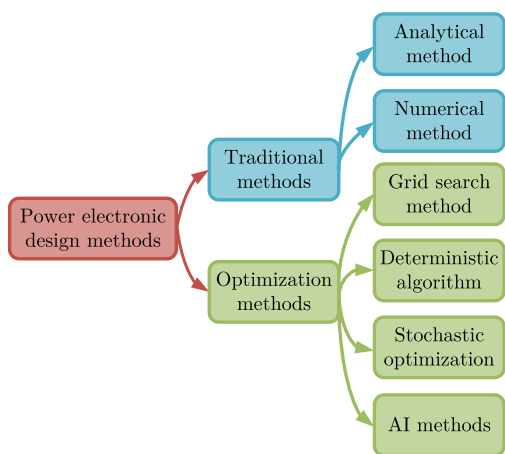

FIGURE. 2. Design methods of power electronics converters.

electronics systems. In [3], the analytical power loss models were used to evaluate the efficiency of the inverter for electric motor and vehicle applications. In [4], the analytical modeling approach was used to identify the power density of a single-phase dual active bridge for aviation application. The model was developed based on the switching frequency and leakage inductance to minimize the total loss and volume of the converter. The analytical models are simple to develop; however, its accuracy of the method was found to be low due to the computational errors through experimental validation against the final prototype. In some traditional methods, mathematical approximations are used to find the analytical expression of optimal designs. For example, the numerical methods include an additional interactive function and an augmented Lagrangian function in the analytical equations to optimize the design accuracy of a switching regulator [5], [6], [7]. Using this method, the converter design can be only optimized for the desired performance and the optimal design parameters are bounded. Also, the order of such mathematical approximation functions cannot be directly determined, which are based on assumptions. These may lead to suboptimal design solutions.

An alternative of traditional approach is the optimization methods. With this method, the combination of design parameters are optimized with respect to the performance parameters of the converter. In [8], [9], [10], a multi-objective optimization method was introduced based on grid search method to identify the Pareto-front of the efficiency and power density of power converters. A design methodology was presented to optimize the losses associated with the medium frequency transformer [11]. These methods are relatively simple to develop for component-level design, but the number of design parameters increases exponentially with the number of variables. The deterministic algorithm computes the mathematical functions of the design and performance parameters of the optimization problems. The mathematical function produces the output for a given objective function [12]. In [13], [14], [15], [16], GP-based optimization approaches were presented to optimize converters power loss and volume. A simplex deterministic approach was presented in [17] to optimize the components of a Cuk converter. However, the deterministic algorithms required additional constraints to converge to the optimal solutions, which increases the complexity. The stochastic optimization methods are based on mathematical functions with random variables, which have been used in power electronic system design. A genetic algorithm (GA) and particle swarm optimization (PSO) based constrained optimization framework were presented to understand the trade-off involved in the converter design [18], [19], [20], [21]. The PSO algorithm is notable for its quick convergence rate and simple implementation. However, the accuracy of PSO algorithm can be reduced by the premature convergence problem due to linearly distributed delays. In [22], a randomly distributed delay was introduced to deal with the convergence problem for a resonant converter design. The complexity of these optimization methods are higher due to the large number of constraints and iterations. Also, the optimal solutions can be diverged due to the random variables.

Artificial intelligence (AI) methods are used to compute the optimal design of power converter without randomization. The soft switching performance and the improved efficiency of power converters can be achieved by the triple phase shift (TPS) modulation techniques. The performance of a TPS scheme was further improved in [23], [24] for a dual active bridge converter using an AI-based automated approach. In [25], a batch-normalization-ANN was introduced to improve the prediction accuracy of the power converters design circuit parameters. However, ANN was only used in the analysis or decision stage of the design, which limits the full potential of ANN methods. In [26], an ANN-based design method was introduced to develop the reliability model for the single-phase inverters. The reliability model was developed by considering the switches and AC filters of the systems. Using this method, high accuracy, reduced computational time, and improved competence can be achieved. The potential of ANN was used to model and optimize the inductor of DC-DC converters [27] with proven improvement of accuracy and reduction of computation time. Also, the ANN was used to
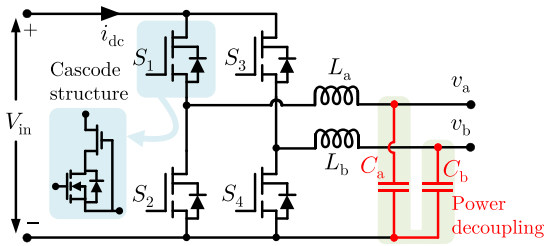
FIGURE. 3. Single-phase inverter with power decoupling.

solve the predictive control challenges of power electronics converters [28]. However, ANN was understudied for the system-level design of converters and few research fully realized the potential of using ANN to design power converters. To bridge this gap, in this paper, an ANN-based multi-objective design approach is proposed and demonstrated by design of a wide-bandgap single-phase inverters. The ANN was trained using the mathematical models of power loss and volume of the switches, heat sinks, inductors, and capacitors of the inverters. The design parameters were the input of ANN, and the performance space parameters were the output (target) of ANN. The back-propagation training algorithm was used to train the network. The well-known Levenberg-Marquardt optimization method updated the weights and bias values. Different data were used for training, validation and testing of the network. The ANN-based design results were verified in efficiency and power density, and compared with designs generated by the numerical model and GP methods. The proposed approach was verified using a 1 kW Gallium Nitride (GaN) inverter prototype. Also, the computational speed of the ANN was compared with the numerical model and GP by changing the number of designs.

II. AN OVERVIEW OF ARTIFICIAL NEURAL NETWORK (ANN)-BASED DESIGN METHOD

The inverter topology that is used to explore the ANN-based design approach is given in Fig. 3. Two identical DC-DC buck converters are used to form the inverter [29]. Each converter will generate the AC voltage with an DC offset and the sinusoidal output voltage is generated by combining both of the converter outputs. Moreover, it can achieve the power decoupling function, eliminating the second-order ripple on the DC-link without adding extra active or passive components.

Fig. 4 shows the workflow of ANN-based design of a single-phase inverter. The first step is to generate the training data set and the data set is fed to the feed-forward network. The training will take several iterations. Once finished, a well-trained ANN will then produce the Pareto-front curve of efficiency and power density fast and accurately, according to the given inputs including switching frequency f_{sw}, the inductor ripple $\triangle i_L$, the switch area A_{sw}, and the junction temperature $\triangle T_j$ (see the blue dash block). A certain design

can then be selected on the Pareto-front and the design components can be selected accordingly to match the input in order to get the desired efficiency and power density. Finally, the prototype will be made using the selected design components.

In this study, four major components of the inverter are considered for the ANN-based design, including the power GaN FETs, inductors, capacitors, and heat sinks. Then, the mathematical models representing the relationship between the input variables (e.g., f_{sw}) and output efficiency and power density have been developed in [30] and hence are not repeated in this paper. Such mathematical models are used to generate the training data sets of ANN and detailed steps are as follows.

1) Define the maximum input voltage $V_{in,max}$, input current $I_{in,max}$, output voltage $V_{out,max}$, and output current $I_{out,max}$ of the inverter
2) Initialize the reference values of the design space constants, output capacitance C_{oss}^*, gate charge Q_g^*, reverse recovery charge Q_{rr}^*, on-state resistance $R_{DS,on}^*$, switch area A_{sw}^*, and thermal resistance junction-case $R_{\theta JC}^*$. These values can be found in the data sheets of GaN FETs.
3) Define the input variables of design method. Then, initialize the minimum and maximum boundary of the input variables $f_{sw,min}$, $f_{sw,max}$, $\triangle i_{L,min}$, $\triangle i_{L,max}$, $A_{sw,min}$, $A_{sw,max}$, $\triangle T_{j,min}$, $\triangle T_{j,max}$.
4) Define the input value and start the iterations.
5) At the end of each iteration, calculate the power loss and volume corresponding to each set of input values. The switching loss P_{sw}, conduction loss P_{cond}, output capacitance loss P_{coss}, reverse recovery loss P_{rr}, gate loss P_g, and body diode loss P_{bd} are calculated from the GaN FETs. Also, the inductor loss P_{ind} and the capacitor loss are calculated. Similarly, the switch volume vol_{sw}, inductor volume vol_{ind}, capacitor volume vol_{cap}, and heat sink volume $vol_{heat\,sink}$ are determined. The total power loss $P_{tot,loss}$ and volume vol_{tot} are calculated as,

$$P_{tot,loss} = P_{sw} + P_{cond} + P_{coss} + P_{rr}$$
$$+ P_g + P_{bd} + P_{ind} + P_{cap} \quad (1)$$

$$vol_{tot} = vol_{sw} + vol_{ind} + vol_{cap} + vol_{heat\,sink} \quad (2)$$

6) Then, the efficiency η, and power density ρ of the inverter are calculated from the power loss and volume data.
7) Check, if the values are within the required efficiency and power density limits, then store the values.
8) Repeat the steps 4-8 for all the iterations.

The flow chart inside the figure explains the steps of training data set generation. The generated data are feed into the neural network to train the network as per the input and target. Once the network is trained, it can produce the efficiency and power density for any input range. Then, the breakdown of power loss and volume of components is obtained; and the optimal design can then be selected.
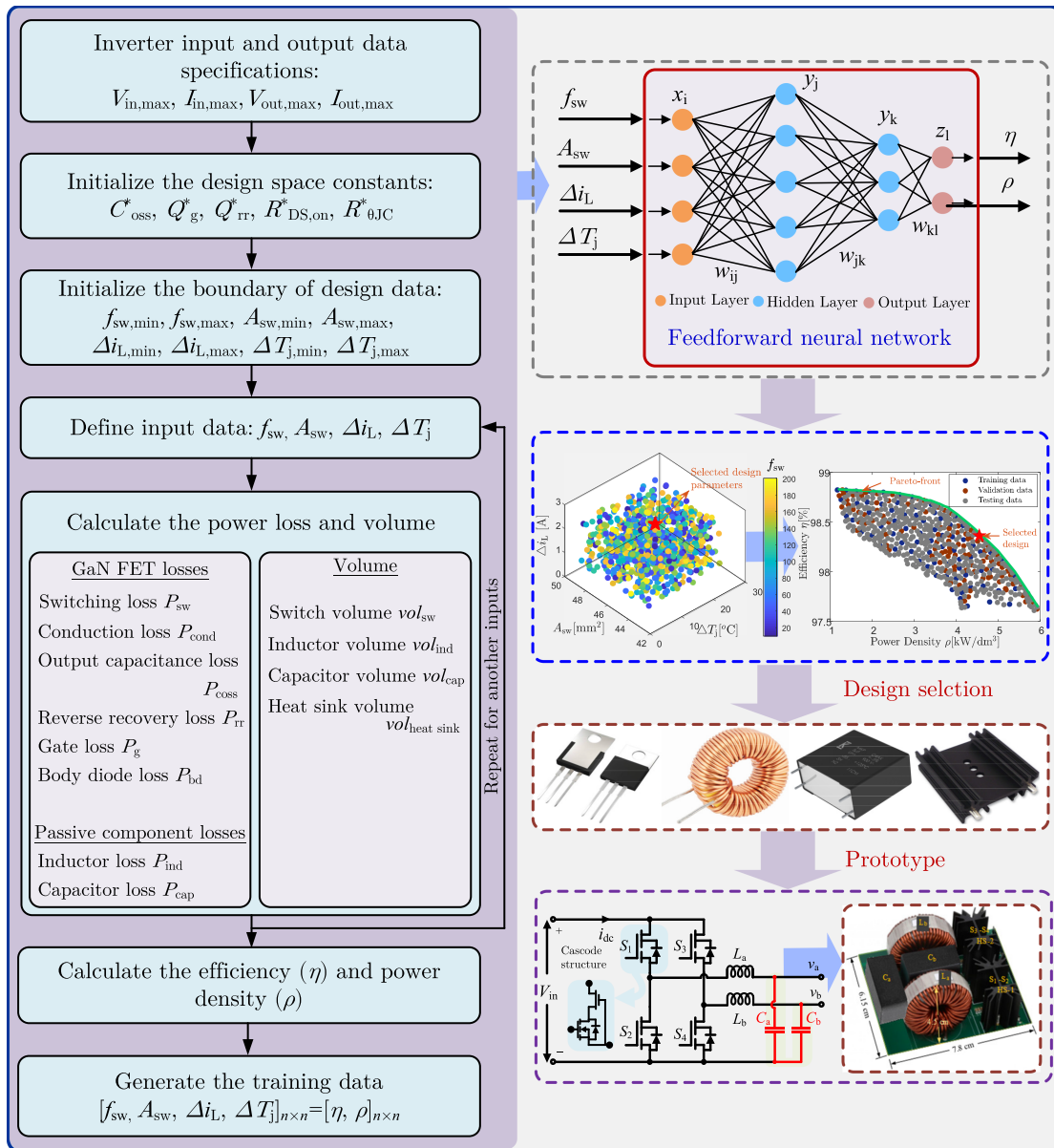
FIGURE. 4. An overview of ANN-based design approach.

III. IMPLEMENTATION OF ANN FOR THE PROPOSED DESIGN

A. STRUCTURE AND LAYERS OF ANN

ANN is one of the AI techniques that can be used to design power converters accurately. It can predict the performance of an inverter based on the design parameters with less computation time. Fig. 5 shows the structure of ANN for the proposed design approach. It consists of three layers: the input layer, hidden layer, and output layer. The layers are interconnected through artificial neurons which are called nodes or units. The number of input and output nodes are selected based on the applications. The selection of hidden nodes is complicated, and a proper sensitivity study is required to choose the number of hidden nodes [26].
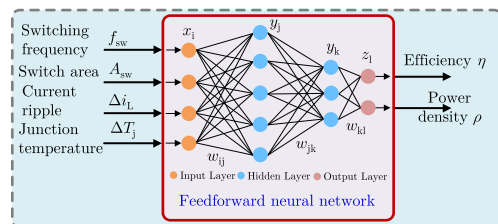

FIGURE. 5. Structure of ANN for proposed design approach.

The complications are that fewer hidden units will reduce the learning ability of the required function. However, this will significantly reduce the training time of the network.

Therefore, proper validation is necessary to ensure network accuracy. The connections between nodes are associated with a weight, which sets the threshold value of each node. The weights between the input and hidden layer are represented as w_{ij}, and the weights between the hidden and the output layer are denoted as w_{jk}. The initial value of the weight is selected randomly between (0,1). Then it will be changed during the training to reach the correct target. The switching frequency f_{sw}, the inductor ripple $\triangle i_L$, the switch area A_{sw}, and the junction temperature $\triangle T_j$ are considered as the input. The efficiency and power density are considered as the target output.

1) INPUT LAYER

The first layer of the network is the input layer which is denoted as x_i, $i = 1, 2 \ldots n$ and can be written as follows.

$$x_i = \begin{bmatrix} f_{sw} \\ A_{sw} \\ \triangle i_L \\ \triangle T_j \end{bmatrix} \tag{3}$$

2) HIDDEN LAYER

The second layer of the network is the hidden layer, which is denoted as y_j, $j = 1, 2 \ldots n$ and y_k, $k = 1, 2 \ldots n$. The hidden layers can be selected in any number, but the computational complexity needs to be considered. The selection of number of hidden layers nodes should consider the trade-off between accuracy and processing time of the network; this is usually obtained by a sensitivity study [27]. The sensitivity study is performed by changing the hidden layer nodes from minimum to maximum number. For every number, the regression of the network is evaluated. Then, the number of hidden layer nodes is finalized for a minimum number with fit ANN. This will improve the accuracy and processing time of the ANN. This will improve the processing time of the ANN. In this paper, two hidden layers are chosen, and the number of neurons in the first and second hidden layers are 5 and 3 accordingly. The weight between the input layer x_i and the hidden layer y_j is represented as w_{ij}; and the weight between the hidden layers y_j and y_k is represented as w_{jk}. The nodes of the hidden layer are made by a threshold function that decides the output of each hidden node. The threshold function can be a step or a tangent sigmoid transfer function. The tangent sigmoid function is used in this paper as,

$$\phi(h) = \frac{1}{1 + e^{-h}} \tag{4}$$

where h is the weighted sum of the input of the hidden nodes. The output of the jth hidden layers is calculated as,

$$y_j = \frac{1}{1 + e^{-\sum_{i=1}^{n} w_{ij} x_i}} = \phi\left(\sum_{i=1}^{n} w_{ij} x_i\right) \tag{5}$$

$$\begin{bmatrix} y_1 \\ y_2 \\ y_3 \\ y_4 \\ y_5 \end{bmatrix}_j = \phi \left(\begin{bmatrix} w_{11} & w_{21} & w_{31} & w_{41} \\ w_{12} & w_{22} & w_{32} & w_{42} \\ w_{13} & w_{23} & w_{33} & w_{43} \\ w_{14} & w_{24} & w_{34} & w_{44} \\ w_{15} & w_{25} & w_{35} & w_{45} \end{bmatrix} \times \begin{bmatrix} f_{sw} \\ A_{sw} \\ \triangle i_L \\ \triangle T_j \end{bmatrix} \right)$$

$$\begin{bmatrix} y_1 \\ y_2 \\ y_3 \\ y_4 \\ y_5 \end{bmatrix}_j = \phi \begin{bmatrix} w_{11} f_{sw} + w_{21} A_{sw} + w_{31} \triangle i_L + w_{41} \triangle T_j \\ w_{12} f_{sw} + w_{22} A_{sw} + w_{32} \triangle i_L + w_{42} \triangle T_j \\ w_{13} f_{sw} + w_{23} A_{sw} + w_{33} \triangle i_L + w_{43} \triangle T_j \\ w_{14} f_{sw} + w_{24} A_{sw} + w_{34} \triangle i_L + w_{44} \triangle T_j \\ w_{15} f_{sw} + w_{25} A_{sw} + w_{35} \triangle i_L + w_{45} \triangle T_j \end{bmatrix}$$

$$\tag{6}$$

Similarly, the output of the kth hidden layers is calculated as,

$$y_k = \frac{1}{1 + e^{-\sum_{j=1}^{n} w_{jk} y_j}} = \phi\left(\sum_{j=1}^{n} w_{jk} y_j\right) \tag{7}$$

3) OUTPUT LAYER

The last layer of the network is the output layer which is denoted as z_l, $l = 1, 2 \ldots n$. In this paper, the efficiency and the power density are considered as the output of the network. The weights between the hidden layer and the output layer are represented as w_{kl}. The computation of the output layer is similar to the hidden layer. The output of the network is calculated as,

$$z_l = \sum_{k=1}^{n} w_{kl} y_k$$

$$\begin{bmatrix} \eta \\ \rho \end{bmatrix} = \begin{bmatrix} w_{11} y_1 + w_{21} y_2 + w_{31} y_3 \\ w_{12} y_1 + w_{22} y_2 + w_{32} y_3 \end{bmatrix} \tag{8}$$

The output of z_k is applied to the tangent sigmoid function to approximate the output within the threshold limits.

B. TRAINING OF THE NETWORK

Training is an iterative process for matching the input of the network for the given target. During training, the weight of the network will be adjusted in every iteration to weights the desired targets. The training process includes an optimization approach to find the optimal weight. In this paper, the network is trained by Levenberg-Marquardt back-propagation algorithm [31]. The training consists of four steps: the feed-forward computation, the back-propagation to the output layer, the back-propagation to the hidden layer, and the updating weights. The details of the steps are explained as follows.

1) FEED-FORWARD COMPUTATION

In this step, the network is initialized by the inputs, targets and weights. The feed-forward computation can be realized from the equations (3)-(8). The initial values of the weights are assigned randomly and they will be updated in the next iteration.

At the end of the computation, the evaluated derivatives of the tangent sigmoid function are stored at each unit.

2) BACK-PROPAGATION TO THE OUTPUT LAYER

After the feed-forward computation, the fitness of the network is evaluated using the back-propagation error of the stored value. The back-propagation error of the output layer is calculated as,

$$z_{l,error} = z_{l,out} \left(1 - z_{l,out}\right) \left(z_{l,target} - z_{l,out}\right) \quad (9)$$

where, $z_{l,error}$ is the error of output layer, $z_{l,out}$ is the actual output, and $z_{l,target}$ is the target output. Based on (9), the error of efficiency η_{error} and power density ρ_{error} can be written as,

$$\eta_{error} = \eta_{out} \left(1 - \eta_{out}\right) \left(\eta_{target} - \eta_{out}\right) \quad (10)$$

$$\rho_{error} = \rho_{out} \left(1 - \rho_{out}\right) \left(\rho_{target} - \rho_{out}\right) \quad (11)$$

where, η_{out} and ρ_{out} are the actual output of efficiency and power density. η_{target} and ρ_{target} are the target output of efficiency and power density.

3) BACK-PROPAGATION TO THE HIDDEN LAYER

Now the back-propagation error of the hidden layers y_k and y_j are calculated. The propagated error of each hidden unit must be computed through the possible backward paths. The back-propagation error of the hidden layer y_k is calculated as,

$$y_{k,error} = y_{k,out} \left(1 - y_{k,out}\right) \sum_{k=1}^{n} w_{jk} y_j \quad (12)$$

The back-propagation error of the hidden layer y_j is calculated as,

$$y_{j,error} = y_{j,out} \left(1 - y_{j,out}\right) \sum_{j=1}^{n} w_{ij} x_i \quad (13)$$

4) UPDATING WEIGHTS

The new weights of the network are adjusted based on the values of back-propagation error. The new weights can be determined by the values of the old weights $w_{kl,old}$ and the change of weights. The change of weights is calculated by the partial derivative of the network error with a learning factor. The change of weights and the new weights of the output layer are calculated as,

$$\triangle w_{kl} = \xi \begin{bmatrix} \eta_{error} \\ \rho_{error} \end{bmatrix} y_k \quad (14)$$

$$w_{kl,new} = w_{kl,old} + \triangle w_{kl} \quad (15)$$

The changes of weights of the hidden layers are updated as,

$$\triangle w_{jk} = \xi y_{k,error} y_j \quad (16)$$

$$\triangle w_{ij} = \xi y_{j,error} \begin{bmatrix} f_{sw} \\ A_{sw} \\ \triangle i_L \\ \triangle T_j \end{bmatrix} \quad (17)$$

The new weights of the hidden layers are updated as,

$$w_{jk,new} = w_{jk,old} + \triangle w_{jk} \quad (18)$$

$$w_{ij,new} = w_{ij,old} + \triangle w_{ij} \quad (19)$$

where, ξ is the learning rate that decides the step length of weight correction. Repeat the iterations until the back-propagation error reaches close to zero. After the training process, the fitness of the network is evaluated through statistical measures. Regression analysis is one of the common measures used to assess the accuracy of network. Once the regression analysis is completed, the network can accurately generate the power converter design parameters based on any given values of input.

IV. RESULTS AND DISCUSSIONS
A. TRAINING, VALIDATION AND TESTING OF THE ANN-BASED DESIGN APPROACH

The proposed ANN-based design approach was implemented in MATLAB/Simulink software platform for designing inverters. The ANN needs to be trained once for all to ensure the effectiveness of the design approach. In this study, 2000 design data were obtained from the mathematical modeling of the targeted inverter shown in Fig. 3. For each design, data of the power loss and volume are calculated; then, the corresponding efficiency and power density are obtained [30]. Out of 2000 data, 30% of the data are used for training, 10% are used for validation, and the remaining 60% are used for testing. An iteration of ANN is based on the epoch, which refers to one cycle of full training of ANN using all the 30% of training data. The proposed ANN-based design took 10 epochs to complete the training, and hence the number of iterations is 10. The regression analysis performances of training, validation, and testing data of and unfit and fit network are given in Fig. 6(a), 6(b), and 6(c). The legend Y represents the fitness of the output and T is the target of the network. If Y equals to T, then the actually output fully matches the desired output and the fitness value R will be 1, indicating a fully linear correlation. For a fit ANN, the fitness value R is 1, and hence this ensures the given structure of ANN is sufficient to produce accurate output. For an unfit ANN, the training fitness value is 0.86, which produces lower fitness values for validation and testing. However, adding more hidden layer nodes extends the learning capabilities of ANNs, which allows the processing of more complex data. If the fitness of the ANN is not sufficient, the number of hidden layers and the number of neurons of the ANN structure can be updated.

The performance of the proposed design methods is then predicting the accurate output for the given input design parameters, including f_{sw}, $\triangle i_L$, A_{sw}, and $\triangle T_j$ as presented in section III. Multiple design combinations are generated to identify the best design for the inverter. Then, the combinations of design parameters are applied to the network, and the corresponding performance parameters are mapped into a 2D space. The Pareto-front response is plotted using these performance parameters, and the trade-off between the
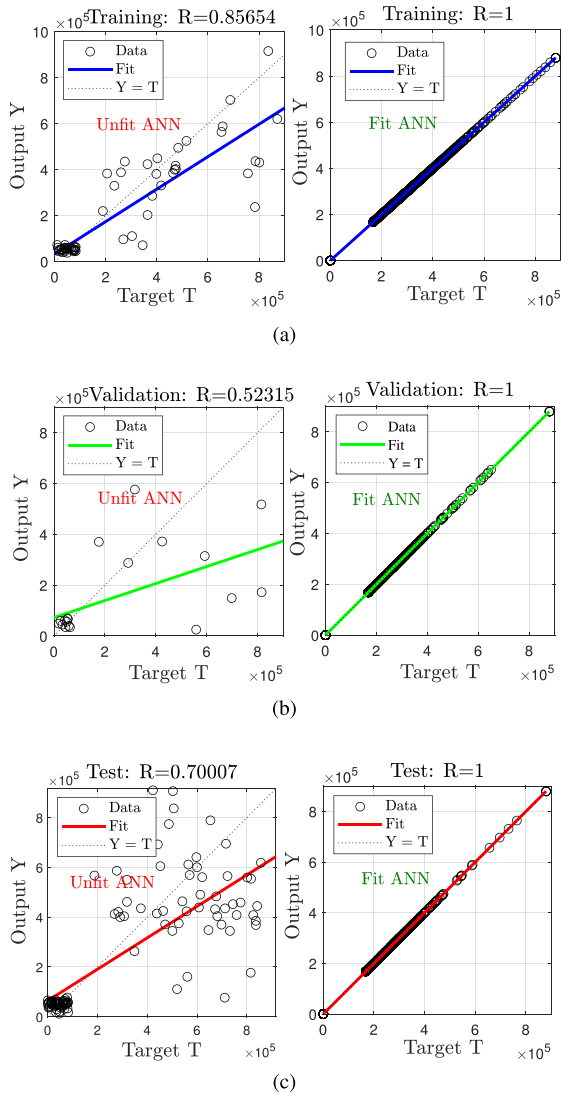
FIGURE. 6. Regression of the network (a) Training (b) Validation and (c) Testing.

TABLE 1. Single-Phase Inverter Implementation Parameters

Parameter	Value
Input voltage V_{in}	450 V
RMS output voltage v_{ab}	230 V
RMS output current i_a	4.35 A
Output capacitor ripple $\triangle v_c$	0.5 V
Ambient temperature $T_{amb.}$	25°C
Maximum junction temp. $T_{j,max}$	50°C
Maximum change of temp. $\triangle T_{j,max}$	25°C

TABLE 2. Design Variables of the Inverter

Design variable	Min. value	Max. value
Switching frequency f_{sw}	30 kHz	200 kHz
Current ripple $\triangle i_L$	$0.1 I_{out.max}$	$0.45 I_{out,max}$
Switch area A_{sw}	$0.94 A_{sw}^*$	$1.07 A_{sw}^*$
Change of junction temp. $\triangle T_j$	1°C	25°C

FIGURE. 7. (a) Input data and (b) Efficiency vs. Power density.

efficiency and power density is obtained. The obtained Pareto-front response is provided with a significant degree of freedom to choose the optimal design parameters such as switching frequency, the value of the passive components and the semiconductor area.

B. INVERTER DESIGN AND PERFORMANCE EVALUATION

In this paper, the performance of the proposed design methods is examined by fast and accurately designing a 1 kW inverter with optimized trade-off between its efficiency and power density. The implementation parameters of the inverter are given in Table 1. The constraints of design variables are given in Table 2. The mathematical models are then executed to generate 2000 designs. In the 2000 data sets, 30% of the data are used for training, which corresponds to reduced usage of mathematical models compared to the numerical model and GP method. For any new design, the ANN does not need to

be trained repetitively and does not require the use of the mathematical model again. Fig. 7(a) shows the 2000 sets of input data of A_{sw}, $\triangle i_L$, $\triangle T_j$, and f_{sw} (color coded) that were used to train, validate, and test the neural network. The output trade-off of efficiency and power density of the power inverter are given as colored data in Fig. 7(b). The Pareto-front is clearly presented as the boundary of the space formed by all the data. Any data on the Pareto-front can be selected to represent one of the best trade-off options that the inverter can
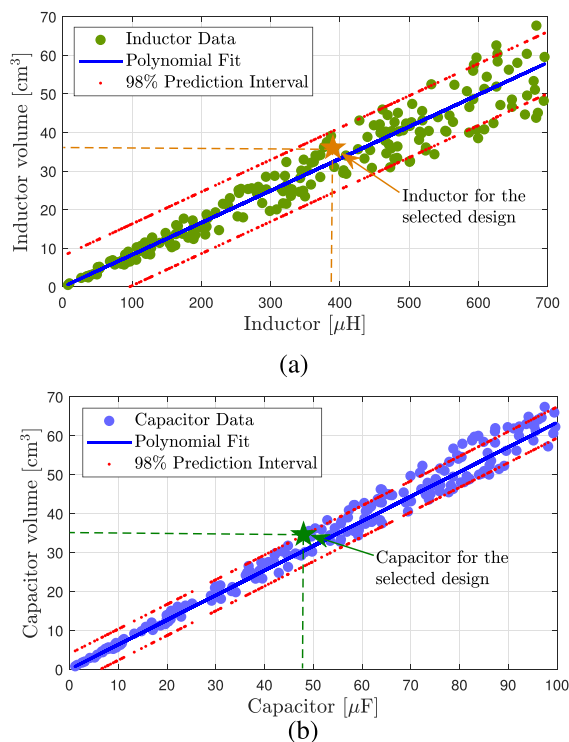
FIGURE. 8. Boxed volume of (a) Inductance and (b) Capacitance.

FIGURE. 9. (a) Volume and (b) Power loss.

TABLE 3. Comparison of Different Design Methods

Design methodologies	Efficiency (%)	Power density (kW/dm^3)
Numerical model	98.30	4.56
GP	98.41	4.50
ANN	98.40	4.57
Experiment	98.02	4.54

achieve. For practical applications, the selection of trade-off would further rely on whether the efficiency is prioritized over power density or vice visa, a particular data (i.e. trade-off) on the Pareto-front can be then selected accordingly.

To validate the proposed method, one design with a best trade-off of $\eta = 98.4\%$ and $\rho = 4.57\,\text{kW/dm}^3$ is selected (see Fig. 7(b)) considering for applications of domestic solar PV inverters. Commercialized domestic inverters typically claim a maximum efficiency between 97% to 98% with a relatively low power density and hence such trade-off would make the designed inverter technically competitive and commercially viable. For the corresponding design, the switching frequency is obtained as $f_{\text{sw}} = 100\,\text{kHz}$. Four 900 V TP90H180PS Transphorm GaN FETs [32] were used to build the proto-type. The inductor and capacitor values are computed to be $L = 390\,\mu\text{H}$ and $C = 48\,\mu\text{F}$ for the selected design, according to Fig. 8(a) and (b). Using the polynomial curve fitting method, the best fitting results are obtained. To improve the design freedom, the design selection region is expanded by estimating the standard error σ. The polynomial fit calculates the value of standard error σ. From that, 98% of the prediction interval is chosen and is calculated as follows.

$$vol_{\text{ind}} \pm 2\sigma \text{ and } vol_{\text{cap}} \pm 2\sigma \qquad (20)$$

The prediction interval improves the design flexibility and helps the designer to select required volume of the inductor and capacitor. The inductor current ripple and the switching frequency are related to the inductor and capacitor values. Based on these parameters, the volume of these components
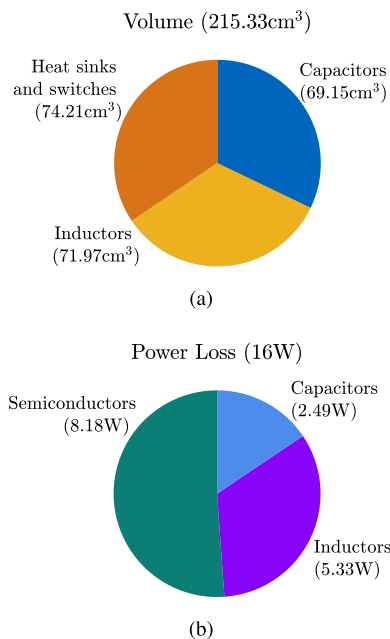
is computed from the ANN output. In this paper, the boxed volume of the inductor and capacitor are obtained as 35.9 cm^3 and 34.6 cm^3. Based on the above selections, two P11T60 series of high current toroid through-hole type fixed copper coil inductors were used which were designed by MPS Industries [33] and two MKP1848 C series of polypropylene film capacitors are used from the Vishay BC Components [34], two extruded radial fins type heat sinks are used from the Aavid [35] for further prototyping the inverter. Symmetrical components are used in both legs of the inverters. Hence, the value, volume, and power loss of both the legs inductor and capacitor are identical. The tolerance of the performance indices is selected based on the industrial design limits.

To conclude, the volume and power loss are obtained as 215.33 cm^3 and 16 W. The breakdown volume and power loss of each component are summarized in Fig. 9(a)–9(b). With the total power losses 16 W, switches contributed 51.13%, inductors 33.31% and capacitors 15.56%. Likewise, with the total volume of 215.33 cm^3, heat sinks and switches counted for 34.46%, inductors 33.42%, and capacitors 32.12%. In Table 3, the efficiency and power density of the proposed ANN method is compared with the existing numerical mod-eling, GP methods and experiment for a selected design.
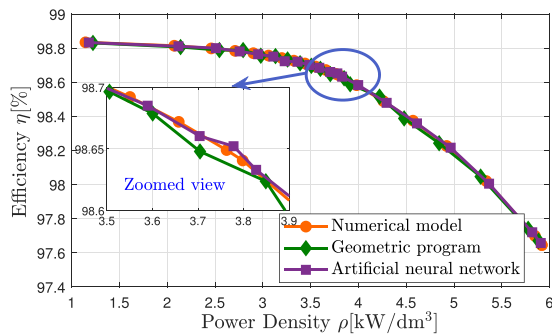
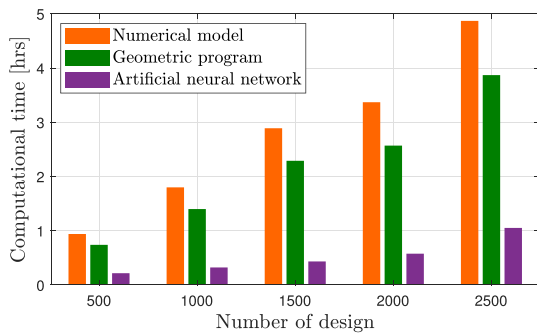FIGURE. 10. Performance space comparison of different methods.

FIGURE. 11. Comparison of computational time with existing methods.

FIGURE. 12. Single-phase inverter prototype with GaN device.

The result of the proposed method is matched closer to the numerical model and experiment than the GP method. The numerical model is the most accurate model which is fully based on mathematical derivations. However, when comparing the aspects of computational time, the ANN-based design method is far better than the other two methods (see Fig. 11 for detailed comparisons on computation time).

C. COMPARISON OF ACCURACY OF ANN TO EXISTING DESIGN METHODS

The accuracy of the ANN-based design approach is compared to the numerical model and GP method. Twenty different designs on Pareto-front obtained by per method are used for comparison as shown in Fig. 10. Within these, the numerical model was purely developed based on mathematical models and hence is considered as the benchmark for the comparison. It can be observed the designs obtained by different methods match well in general, especially when the power density is larger than $4\,\text{kW/dm}^3$. However, some mismatches can be observed when the designed power density is lower (e.g., see the zoomed view). The average mismatch of twenty different designs are then calculated to obtain the accuracy of different design methods. The ANN method has an accuracy of 97.3% when compared to the numerical model, i.e. an average mismatch of 2.73% over the twenty designs; while the accuracy of GP method is only 88.63% with an average mismatch of 11.37%. Hence, the ANN-based design method is more accurate than the GP based design method. In addition, it is worth
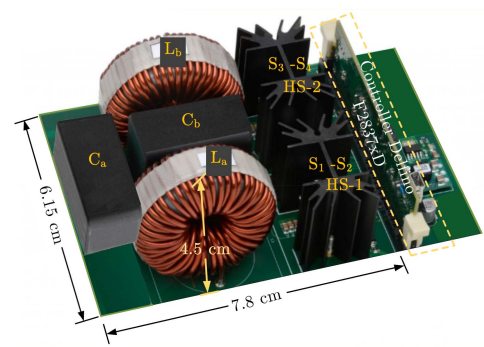
mentioning the accuracy of ANN remains similarly high for obtaining designs not on the Pareto-front (e.g., data that are not on the Pareto-front in Fig. 7(b)) while the GP methods become more inaccurate for those designs.

D. COMPARISON OF COMPUTATIONAL TIME OF ANN TO EXISTING DESIGN METHODS

The computational time of the proposed ANN-based design approach is compared with the numerical model and GP method. The computational time was measured by running each design approach on a computer with the processor Intel(R) Core(TM) i7-6500 U CPU @ 2.50 GHz and the installed RAM 16.0 GB. Five sets of different numbers of designs (500, 1000, 1500, 2000, and 2500) are chosen to validate and compare the computational time of different approaches. Th results are given in Fig. 11. It is pretty obvious that the computational time of ANN-based method is much shorter than the GP-based method and numerical modeling. Such advantages become more significant with the increase of number of design. For 2500 designs, the numerical modeling takes 4 hrs and 56 mins, the GP approach 3 hrs 52 mins to complete the computation of all the designs. Instead, the ANN-based approach only takes 1 hr 15 mins, which is about 78% and 67% shorter than numerical modeling and GP-based method respectively. Such a faster speed of ANN is a result of avoidance of repetitive progress of mathematical models. The training of ANN is done once for all with a limited number of iterations. For any new design, the ANN does not need to be trained repetitively. However, for the numerical model and GP method, mathematical models of the inverters with new input will need to be repeated every time and this contributes significantly to the computational complexity.

E. EXPERIMENTAL VERIFICATION

Experimental assessment was done to verify the selected design obtained by the ANN-based approach, aiming at an efficiency of 98.4% and a power density of $4.57\,\text{kW/dm}^3$ (see Fig. 7(b)). The design was compared to the fabricated 1 kW hardware prototype. Fig. 12 shows the single-phase inverter prototype with control cards (Delfino F2837xD) and the sensors. The current sensor ACS723 is highly accurate,
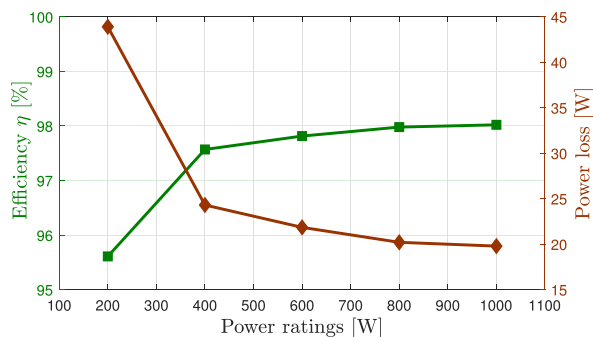
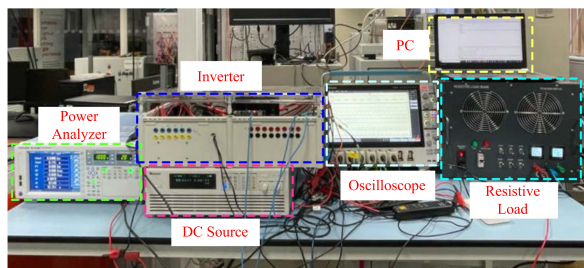**FIGURE. 13.** Efficiency and power losses of the hardware.

FIGURE. 14. Experimental setup of single-phase differential buck inverter.

FIGURE. 15. Steady-state performance of 1 kW inverter design [V_{in}], V_{Ca}, V_{Cb}: 200 V/div, i_{dc}: 5 A/div, i_a: 10 A/div, v_{ab}: 300 V/div].

galvanically isolated current sensor IC, and a voltage divider circuit is used to feedback the voltage to the controller, both of which are in the bottom layer of the board. The switches, heat sinks, inductors and capacitors were not changed in the experiments and hence no extension board is needed. The prototype was examined at different output power levels to obtain its efficiency and power loss which are shown in Fig. 13. Yokogawa WT1806E precision power analyzer was used to measure the efficiency. It can be observed that the efficiency of the prototype at 1 kW is 98.02%. The power density is obtained as 4.54 kW/dm^3 from the volume of the inverter. Therefore, the experimental efficiency and power density matches well with the selected design obtained by the ANN-based approach. The errors of efficiency and power density are only 0.38% and 0.03 kW/dm^3 respectively.

Additional tests were undertaken to showcase the smooth operation of the designed single-phase differential inverter. Fig. 14 shows the experimental setup where the single-phase differential buck inverter was connected to a DC voltage source (Chroma 62000H-S Series) and to an AC load bank (FFLB-5 kW). The inverter operated to reduce the second-order ripples of its DC current (i.e. power decoupling function). Fig. 15 shows the experimental results of input voltage V_{in}, dc-link current i_{dc}, output voltage v_{ab}, output current i_a, and decoupling capacitor voltages V_{Ca}, V_{Cb}. The second-order ripple of DC current (in teal blue) was reduced from 2.25 A (see Fig. 15 (Zoom A)) to 0.27 A (see Fig. 15 (Zoom B)) by enabling a ripple controller. Such a function is an inherent advantage of differential buck inverter to avoid using bulky
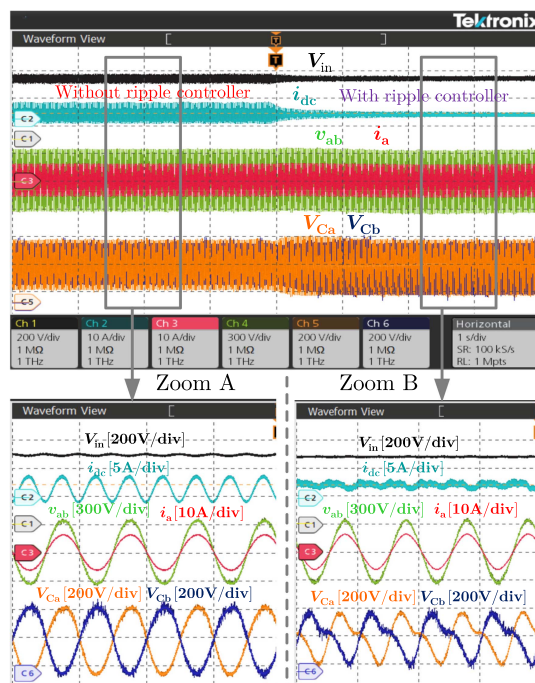
DC-link electrolytic capacitors and hence benefits the reliability and size of the inverter. This is not directly linked to the ANN-based design but rather to further justify this type of inverter, as a good example to be used to demonstrate the design process based on the ANN-based approach.

V. CONCLUSION

An ANN-based design approach has been proposed to enhance the design performance of wide-bandgap power electronics converters. The ANN can be easily trained using a back-propagation algorithm and then be applied for the design process. The approach generates optimal designs located on the efficiency - power density Pareto-front curve. This ensures the best trade-off between the output performance parameters and allows the designer to quickly identify the required design parameters to fabricate inverters with such optimal designs.

The proposed method has significant advantages in the reduction of computation time. It reduces around 78% and 67% computation time compared to the numerical model and GP methods when processing 2500 design cases. Hence, more processing time will be saved with the increasing number of design cases. The accuracy of the ANN-based design approach is also very high, its design accuracy for twenty designs has been tested to be 97.3% with an average mismatch of 2.73% while the GP method has only 88.63%.

The design approach has been further validated through experimental tests on a GaN-based single-phase inverter which was designed to have an efficiency of 98.4% and a power density of 4.57 kW/dm^3. The tested efficiency and power density are 98.02% and 4.54 kW/dm^3, which well match the designed

values, with an error of 0.38%, and $0.03\,\text{kW/dm}^3$. Thus, the accuracy of the design approach has been validated.

It is foreseeable that the ANN will be gradually used more for converters designs due to the advantages of fast computation and high accuracy, and the presented work is well and timely contributed to this aspect and demonstrates the huge potential of using ANN for converter designs.

REFERENCES

[1] R. M. Burkart and J. W. Kolar, "Advanced modeling and multi-objective optimization/evaluation of SiC converter systems," in *Proc. Tutorial 3rd IEEE Workshop Wide Bandgap Power Devices Appl. (WiPDA)*, 2015, pp. 2–5.

[2] R. M. Burkart and J. W. Kolar, "Comparative η-ρ-σ pareto optimization of Si and SiC multilevel dual-active-bridge topologies with wide input voltage range," *IEEE Trans. Power Electron.*, vol. 32, no. 7, pp. 5258–5270, Oct. 2017.

[3] J. Lai, R. Young, G. Ott, and J. McKeever, "Efficiency modeling and evaluation of a resonant snubber based soft-switching inverter for motor drive applications," in *Proc. PESC '95 – Power Electron. Specialist Conf.*, 1995, vol. 2, pp. 943–949.

[4] N. Fritz, M. Rashed, S. Bozhko, F. Cuomo, and P. Wheeler, "Analytical modelling and power density optimisation of a single phase dual active bridge for aircraft application," *J. Eng.*, vol. 2019, no. 7, pp. 3671–3676, 2019.

[5] S. Balachandran and F. C. Lee, "Algorithms for power converter design optimization," *IEEE Trans. Aerosp. Electron. Sys.*, vol. AES-17, no. 3, pp. 422–432, May 1981.

[6] C. J. Wu, F. C. Lee, S. Balachandran, and H. L. Goin, "Design optimization for a half-bridge DC-DC converter," *IEEE Trans. Aerosp. Electron. Sys.*, vol. AES-18, no. 4, pp. 497–508, Jul. 1982.

[7] T. G. Wilson, E. W. Whelan, R. Rodriguez, and J. M. Dishman, "DC-DC converter power-train optimization for maximum efficiency," *IEEE Trans. Aerosp. Electron. Sys.*, vol. AES-19, no. 3, pp. 413–427, May 1983.

[8] J. W. Kolar, J. Biela, and J. Minibock, "Exploring the pareto front of multi-objective single-phase PFC rectifier design optimization - 99.2% efficiency vs. $7\,\text{kw/din}^3$ power density," in *Proc. IEEE 6th Int. Power Electron. Motion Control Conf.*, 2009, pp. 1–21.

[9] U. Badstuebner, J. Biela, and J. W. Kolar, "An optimized, 99% efficient, 5 kw, phase-shift pwm dc-dc converter for data centers and telecom applications," in *Proc. Int. Power Electron. Conf. - ECCE ASIA*, 2010, pp. 626–634.

[10] I. Laird, X. Yuan, J. Scoltock, and A. J. Forsyth, "A design optimization tool for maximizing the power density of 3-Phase DC-AC converters using silicon carbide (SiC) devices," *IEEE Trans. Power Electron.*, vol. 33, no. 4, pp. 2913–2932, Apr. 2018.

[11] M. Mogorovic and D. Dujic, "100 kW, 10 kHz medium-frequency transformer design optimization and experimental verification," *IEEE Trans. Power Electron.*, vol. 34, no. 2, pp. 1696–1708, Feb. 2019.

[12] R. Yu, B. M. H. Pong, B. W.-K. Ling, and J. Lam, "Two-stage optimization method for efficient power converter design including light load operation," *IEEE Trans. Power Electron.*, vol. 27, no. 3, pp. 1327–1337, Mar. 2012.

[13] A. Stupar, J. A. Taylor, and A. Prodic, "Posynomial models of inductors for optimization of power electronic systems by geometric programming," in *Proc. IEEE 17th Workshop Control Model. Power Electron. (COMPEL)*, 2016, pp. 1–8.

[14] A. Stupar, M. Halamicek, T. Moiannou, A. Prodic, and J. A. Taylor, "Efficiency optimization of a 7-Switch flying capacitor buck converter power stage IC using simulation and geometric programming," in *Proc. IEEE 19th Workshop Control Model. Power Electron. (COMPEL)*, 2018, pp. 1–8.

[15] A. Stupar, T. McRae, N. Vukadinovic, A. Prodic, and J. A. Taylor, "Multi-objective optimization of multi-level DC-DC converters using geometric programming," *IEEE Trans. Power Electron.*, vol. 34, no. 12, pp. 11 912–11 939, Dec. 2019.

[16] R. Rajamony, S. Wang, R. Navaratne, and W. Ming, "Multi-objective design of single-phase differential buck inverters with active power decoupling," *IEEE Open J. Power Electron.*, vol. 3, pp. 105–114, 2022.

[17] R. Leyva, "Optimal sizing of cuk converters via geometric programming," in *Proc. IECON 42nd Annu. Conf. IEEE Ind. Electron. Soc.*, 2016, pp. 2480–2485.

[18] D. Malyna, J. Duarte, M. Hendrix, and F. van Horck, "Multi-objective optimization of power converters using genetic algorithms," in *Proc. Int. Symp. Power Electron., Elect. Drives, Automat. Motion*, SPEEDAM, 2006, pp. 713–717.

[19] H. Mejbri, K. Ammous, S. Abid, H. Morel, and A. Ammous, "Multi-objective optimization of power converter sizing based on genetic algorithms: Application to photovoltaic systems," *Int. J. Computation Math. Elect. Electron. Eng.*, vol. 33, no. 1/2, pp. 398–422, 2014.

[20] T. Delaforge and S. Mariethoz, "Design Automation of Power Electronic Converters a Grid Elitist Multiobjective Genetic Algorithm," in *Proc. IEEE Appl. Power Electron. Conf. Expo.*, 2020, pp. 2892–2899.

[21] J. Zhang, Y. Shi, and Z. H. Zhan, "Power electronic circuits design: A particle swarm optimization approach," *Simulated Evol. Learn.*, vol. 34, no. 11, pp. 605–614, Nov. 2008.

[22] F. Lin, X. Zhang, and X. Li, "Design methodology for symmetric CLLC resonant DC transformer considering voltage conversion ratio, system stability, and efficiency," *IEEE Trans. Power Electron.*, vol. 36, no. 9, pp. 10157–10170, Sep. 2021.

[23] F. Lin, X. Zhang, X. Li, C. Sun, W. Cai, and Z. Zhang, "Automatic triple phase-shift modulation for dab converter with minimized power loss," *IEEE Trans. Ind. Appl.*, vol. 58, no. 3, pp. 3840–3851, May/Jun. 2022.

[24] X. Li, X. Zhang, F. Lin, C. Sun, and K. Mao, "Artificial-intelligence based triple phase shift modulation for dual active bridge converter with minimized current stress," *IEEE J. Emerg. Sel. Topics Power Electron.*, early access, Aug. 17, 2021, doi: 10.1109/JESTPE.2021.3105522.

[25] X. Li, X. Zhang, F. Lin, and F. Blaabjerg, "Artificial-intelligence-based design for circuit parameters of power converters," *IEEE Trans. Ind. Electron.*, vol. 69, no. 11, pp. 11144–11155, Nov. 2022.

[26] T. Dragicevic, P. Wheeler, and F. Blaabjerg, "Artificial intelligence aided automated design for reliability of power electronic systems," *IEEE Trans. Power Electron.*, vol. 34, no. 8, pp. 7161–7171, Aug. 2019.

[27] T. Guillod, P. Papamanolis, and J. W. Kolar, "Artificial neural network (ANN) based fast and accurate inductor modeling and design," *IEEE Open J. Power Electron.*, vol. 1, pp. 284–299, 2020.

[28] T. Dragicevic and M. Novak, "Weighting factor design in model predictive control of power electronic converters: An artificial neural network approach," *IEEE Trans. Ind. Electron.*, vol. 66, no. 11, pp. 8870–8880, Nov. 2019.

[29] I. Serban, "Power decoupling method for single-phase H-bridge inverters with no additional power electronics," *IEEE Trans. Ind. Electron.*, vol. 62, no. 8, pp. 4805–4813, Aug. 2015.

[30] R. Rajamony, W. Ming, and S. Wang, "Artificial neural networks based multi-objective design approach for single-phase inverters," in *Proc. IEEE 9th Int. Power Electron. Motion Control Conf. (IPEMC2020-ECCE Asia)*, 2020, pp. 409–416.

[31] B. Hu et al., "Heat-flux-based condition monitoring of multichip power modules using a two-stage neural network," *IEEE Trans. Power Electron.*, vol. 36, no. 7, pp. 7489–7500, Jul. 2021.

[32] "900 V GaN FET (TP90H180PS)," Mar. 2021. [Online]. Available: https://www.transphormusa.com/en/document/datasheet-tp90h180ps-900v-gan-fet/

[33] "High current toroid fixed inductors," Aug. 2018. [Online]. Available: https://magnetic-components.mpsind.com/viewitems/toroidal-fixed-inductors/-p11t60-series-high-current-toroid-fixed-inductors

[34] "Metallized polypropylene film capacitor DC-Link capacitor," Feb. 2022. [Online]. Available: http://www.vishay.com/capacitors/film/

[35] "Board Level Cooling–Extruded 5290," Dec. 2020. [Online]. Available: https://www.boydcorp.com/aavid-datasheets/Board-Level-Cooling-Extruded-5290.pdf

RAJESH RAJAMONY received the M.S. (By Research) degree in electrical and electronics engineering from Anna University, Chennai, India, in 2015, and the Ph.D. degree in electrical and electronic engineering from Cardiff University, Cardiff, U.K., in 2022. He is currently a Power Electronics Application Engineer with Nexperia, Manchester, U.K. His research interests include wide-bandgap power converters, modeling, and design and control of power electronic systems.

SHENG WANG (Member, IEEE) received the B.Eng. degree from Cardiff University, Cardiff, U.K. and North China Electric Power University, Beijing, China, in 2011, and the Ph.D. degree from Cardiff University, in 2016. He was a Research Assistant, from 2013 to 2014, a Research Associate from 2016 to 2018, and a KTP Associate from 2018 to 2020 with Cardiff University, where since 2020, he has been a Lecturer with the School of Engineering. His research interests include control and protection of HVdc and MVdc, power electronic devices, and compound semiconductor.

INGO LUDTKE received the Dipl.Ing. (FH) degree in electrical engineering/computer science from Fachhochschule Braunschweig/Wolfenbüttel, Wolfenbüttel, Germany, in 1990, the Dipl.Ing. (TH) degree in electrical engineering/automation technology from Technische Hochschule Zwickau, Zwickau, Germany, in 1991, and the Ph.D. degree in electrical engineering from the University of Glamorgan, Pontypridd, U.K., in 1998. He is currently the Head of the Power Electronics of Compound Semiconductor Applications Catapult, Newport, U.K. His research interests include motor control, optimization, modeling, and applications of wide bandgap compound semiconductor power devices. He was the recipient of the title of Honorary Visiting Professor from Cardiff University, Cardiff, U.K., in 2020.

GERARDO CALDERON-LOPEZ received the B.Sc. degree in communications and electronics engineering from the National Polytechnic Institute, Mexico City, Mexico, in 1999, the M.Sc. degree in power electronics and drives from the University of Birmingham, Birmingham, U.K., and University of Nottingham, Nottingham, U.K., in 2001, and the Ph.D. degree in power electronics from The University of Manchester, Manchester, U.K., in 2009. He was a Research Associate with The University of Manchester. He is currently a Senior Power Electronics Engineer with Compound Semiconductor Applications Catapult, Newport, U.K. His research interests include power-dense converters and magnetic components.

WENLONG MING (Member, IEEE) received the B.Eng. and M.Eng. degrees in automation from Shandong University, Jinan, China, in 2007 and 2010, respectively, and the Ph.D. degree in automatic control and systems engineering from the University of Sheffield, Sheffield, U.K., in 2015. Since August 2020, he has been a Senior Lecturer of Power Electronics with Cardiff University, Cardif, U.K., and since April 2020 has been a Senior Research Fellow funded by Compound Semiconductor Applications Catapult, Newport, U.K., for 5 years. He was with the Center for Power Electronics Systems, Virginia Tech, Blacksburg, USA, in 2012, as an Academic Visiting Scholar. He has coauthored more than 60 papers published in leading journals or refereed IEEE conferences. His research interests include packaging, characterisation, modeling and applications of wide-bandgap semiconductor power devices. He was the winner of the prestigious IET Control & Automation Doctoral Dissertation Prize in 2017.